Hindawi Publishing Corporation
International Journal of Inorganic Chemistry
Volume 2011, Article ID 108087, 8 pages
doi:10.1155/2011/108087

*Research Article*

# Surfactant-Assisted Sol-Gel Synthesis of $TiO_2$ with Uniform Particle Size Distribution

**O. L. Galkina,[1,2] V. V. Vinogradov,[1] A. V. Agafonov,[1] and A. V. Vinogradov[2]**

[1] *Institute of Solution Chemistry, Russian Academy of Sciences, ul. Akademicheskaya 1, Ivanovo 153045, Russia*
[2] *Ivanovo State University of Chemistry and Technology, pr. Engel'sa 7, Ivanovo 153000, Russia*

Correspondence should be addressed to O. L. Galkina, olgalgalkina@mail.ru

Received 8 November 2011; Accepted 18 December 2011

Academic Editor: James McCusker



$TiO_2$ materials were prepared from a titanium isopropoxide precursor by sol-gel processing in water media with or without various templates (polyethylenimine or Pluronic P-123). The photocatalytic efficiency of the samples was found to depend strongly on the use of and type of template added. Titania/Pluronic sols resulted in homogeneous anatase $TiO_2$—rutile with uniform particle size distribution after calcination (400°C). Optical properties of the samples were characterized by UV-Vis spectroscopy and crystalline structures by X-ray diffraction. A surfactant-assisted sol-gel process retarded crystallization of the anatase and rutile titania, which resulted in smaller grain sizes and presumably a larger active surface area. The morphology of the surfaces was obtained by AFM techniques. The highest photobleaching rate was found for samples deposited from the sol with the addition of the Pluronic P-123 surfactant, and it was almost twice as high as that for films deposited from sols with polyethylenimine.

## 1. Introduction

Titania coatings with high specific surface area and with narrow pore size distribution have a big prospect of practical application in such areas as solar energy transformation [1] and photocatalysis [2–7] for water and air clearing and processing, as self-cleaning coatings for windows and tiles [8]. The pore size and specific surface area substantially affect the physical properties of these materials and can play a significant role in their activity. For example, catalytic application demands an adjustable porosity for optimization of rate of reagent diffusion towards adsorption centers and a large surface area for the maximum interaction between the reagent flow and the catalyst surface.

Titania-based coatings can be synthesized by various methods, but sol-gel process is the most applied as this method possesses some advantages, such as homogeneity at molecular level, a wide range of a precursor selection, control over microstructure, low demands upon reagent purity, possibility of a fine adjustment of the end product properties, simplicity of process, and low temperature and cost.

Synthesis of titania by sol-gel method is usually attained by hydrolysis of titanium alkoxide precursors. Nevertheless, two various approaches can be applied accordingly to process parameters. So far, the most widespread [9–18] is the polymeric approach where an alcohol usually acts as a solvent, and hydrolysis is carefully controlled by means of the limited quantity of water. As a rule, an acid catalyst (HCl and $HNO_3$) is therewith used, which forms a complex with alkoxide, thus making the decrease in the hydrolysis reaction rate possible. This method leads to formation of amorphous films, which should be exposed to thermal processing to form crystal phase.

In the second case, the solvent is water which is added in large excess to alkoxide. In these conditions hydrolysis proceeds very rapidly, and its products are superfine primary particles whose size fluctuates from 2 to 8 nanometers [19]. These nanoparticles are agglomerated very quickly, giving large aggregates of macroscopical sizes [20]. Peptization by means of inorganic acids (HCl and $HNO_3$) is used to destroy the aggregates and to obtain colloidal suspensions containing particles whose size fluctuates from 15 to 100 nanometers. Thus, the second approach utilizes cheap and nontoxic solvents (water), making it possible to obtain materials with crystal phase for direct application as coatings with low thermal stability (polymers). It is this approach that has been studied in this work.

Thus, the goal of this research was the search for corresponding parameters of synthesis process, which are necessary for simple preparation of highly stable titania hydrosols in water medium in the presence of organic templates for obtaining the titania-based materials with high photocatalytic activity. The present work describes the parameters of water medium sol-gel synthesis of mesoporous titania obtained using various types of templates. The advantages of the synthesized materials in the process of photocatalytic decomposition of a model dye compared to an industrial Hombikat sample are shown.

## 2. Experimental

*2.1. $TiO_2$ Preparation.* The $TiO_2$ nanoparticles were prepared by sol-gel synthesis in water medium. For preparation of the $TiO_2$ nanoparticles, the following materials were used: titanium tetraisopropoxide (Aldrich, 97%) as a precursor, the concentrated hydrochloric acid (37%), bidistilled water, polyethylenimine ($M_w$ = 25000, $M_n$ = 10000), and Pluronic P-123. The synthesis was carried out in the conditions of continuous stirring at the temperature of 50°C. All reactants were purchased in Sigma-Aldrich.

The concentrated HCl (1.86 mL) was added to the conic flask containing 50 mL of bidistilled water. Then, the water-acid mixture (pH = 1-2) was dosed at continuous stirring with 30 mL of titanium tetraisopropoxide (TTIP) in small portions. The white and dense precipitate was formed and gradually peptized after 3 hours to form a transparent sol. Then, the obtained sol was dosed with 3 g of a template (polyethylenimine or Pluronic P-123), leading to the formation of a gel which was dried in the air at the temperature of 60°C. For removal of the organic part, the dried samples were calcinated at the temperature of 400°C for 4 hours.

*2.2. Materials Characterization.* Sols and template solutions were characterized in particle size by dynamic light scattering technique using Malvern ZetaSizer Nano at 20°C with a 10 mW He-Ne laser, 633 nm wavelength, and 90° fixed scattering angle.

Crystal structure of calcinated samples was determined by X-ray diffraction with a Bruker Nanostar U diffractometer using CuK a radiation (1.54 Å).

Since the brookite disappears at temperatures higher than 400°C, the mass fraction of rutile phase of powders annealed higher than that temperature can be calculated by the following equation [21]:

$$\chi_{\text{rutile}} = \frac{1}{1 + K(I_A/I_R)}, \tag{1}$$

where $I_A$ is the intensity of the anatase reflection and $I_R$ is that of the rutile (110). The empirical constant $K$ was determined via an XRD analysis of powders of known proportions of pure anatase and pure rutile and is equal to 0.79.

The anatase content of powders annealed at temperatures lower than 400°C was estimated by the following equation:

$$\text{anatase} = \frac{\sum_1^N I_{A_i}}{\sum_1^N I_{A_i} + \sum_1^N I_{B_j}}, \tag{2}$$

where $I_{A_i}$ is the intensity of the anatase reflections and $I_{B_j}$ is the intensity of the brookite reflections.

The crystallite size was calculated using the Scherrer equation:

$$D = \frac{k\lambda}{B\cos\theta}, \tag{3}$$

where $k$ is the constant equal to 0.94, $\lambda$ is the X-ray wavelength, $B$ is half-width at half-maximum, and $\theta$ is the diffraction angle of the phase under investigation.

Atomic force microscope (AFM) studies were carried out using a SPM Solver P47H-PRO microscope. Samples were applied on glass plate having clean surface.

BET surface areas of the samples were calculated from nitrogen physisorption data collected on a Quantachrome Nova 1200 Series-e analyzer at 77 K. The pore size distributions were calculated using the BJH method from the desorption branch of the isotherms.

EVM-100L transmission electron microscope was used to determine porous morphology. The samples were prepared by sonicating 10 mg of sample in 10 mL of ethanol. One drop of the suspension was placed on a carbon copper grid and allowed to dry completely. Accelerating voltage was 100 keV.

*2.3. Photocatalytic Activity Determination.* Photocatalytic activity of samples was estimated using the reaction of methyl orange decomposition in water solutions. The source of ultraviolet radiation was the high-pressure 250 W mercury lamp with radiation maximum at 365 nm.

The reaction container was an 800 mL cylindrical vessel, in which the water-cooled quartz jacket was located. In the middle of the quartz jacket in its center, the lamp was placed. At the bottom of the reactor, there was a magnetic mixer which provided effective stirring of reaction mass. Air blown through the reaction solution was brought from the bottom to provide constant concentration of the dissolved oxygen. The quantity of the powdery $TiO_2$ was 1 g/L. The initial concentration of methyl orange amounted to 40 mg/L upon the UV irradiation. The temperature of the reaction solution was held at 25 ± 0.5°C. The dyed water probes were collected after different time intervals. The obtained samples were centrifuged, and their absorption spectrum was studied. Residual concentration of methyl orange was determined using a PG Instruments T70 + UV/VIS spectrophotometer at the wavelength of 465 nm. Photocatalytic activity of the obtained samples was compared to that of a Hombikat commercial titania.

## 3. Results and Discussion

*3.1. Optical Properties and Dynamic Light Scattering.* Figure 1 shows the average hydrodynamic size of the $TiO_2$ hydrosol

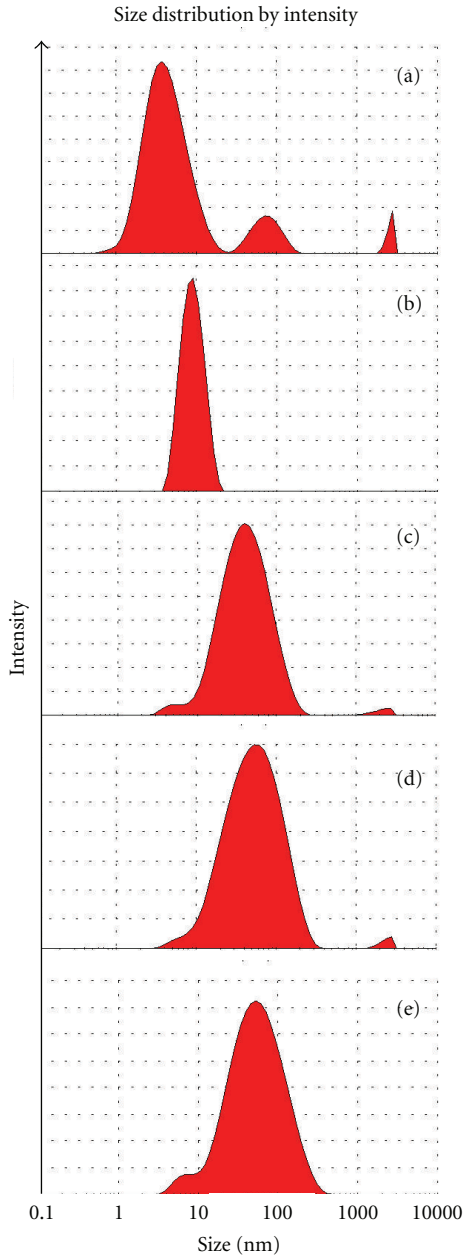


Figure 1: Average hydrodynamic radius: PEI (a), Pluronic P-123 (b), $TiO_2$ (c), $TiO_2$-P123 (d), $TiO_2$-PEI (e).

particles, water solutions of organic templates, and products of their interaction between themselves. Hydrodynamic diameter of titania particles in sols is determined by ionic force of a medium. High molar ratio [$HCl/TiO_2$] and high surface charge around the particles lead to the prevention of coagulation and the precipitation of a flake-like deposit of the $TiO_2$ particles in the presence of organic templates at the expense of electrostatic repulsion. The excess of HCl can compress the double layer in such a way that interaction of particles at a distance decreases during collision, and as a result agglomerates are formed [22].

Therefore, we have chosen the optimum concentration of the hydrochloric acid that is required to split the particles

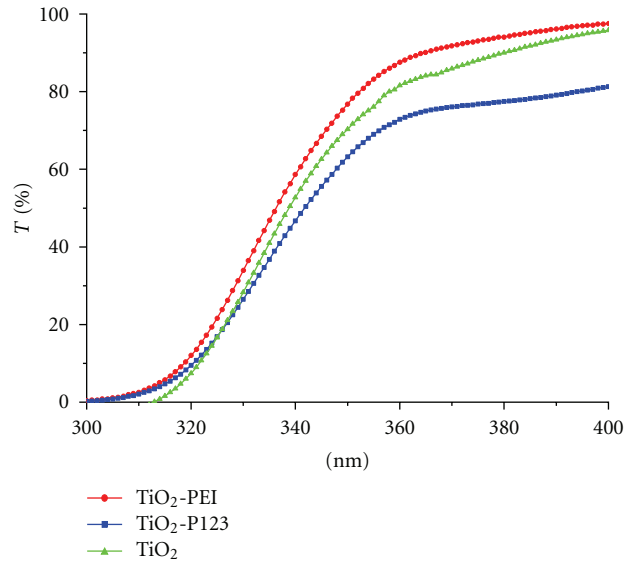


Figure 2: UV-Vis transmittance spectra of $TiO_2$ synthesized films.

into smaller ones during peptization and to prevent coagulation, on the one hand, of the $TiO_2$ particles and, on the other, of the products of interaction of these particles with organic templates. Solutions containing organic templates (Figures 1(a) and 1(b)) have a single maximum in the range of less than 10 nm.

The titania hydrosol particles have an average hydrodynamic radius of about 50 nm (Figure 1(c)), which testifies that individual titania particles interact with each other, forming nanometer agglomerates at the expense of formation of polymeric inorganic chains between themselves. As a result of addition of template organic molecules to the solution containing titania hydrosol, the formation of mesostructures (Figures 1(d) and 1(e)) takes place, where size is approximately equal to the sum of the sizes of titania hydrosol nanoparticles and micellar structures of organic template. The presence of maxima characteristic for individual compounds is not observed.

The visible and UV area transmittance spectra of the calcinated films based on $TiO_2$ containing various templates are presented in Figure 2.

The films were prepared by the method of extraction from corresponding solutions and further calcination on a glass substrate at 400°C and temperature exposure for 4 hours.

The transparency of all films is high, and the films have a transmittance of around 80%. Absorption of photons by the photocatalyst during the catalytic process leads to the excitation of electrons and their transfer from the valence to the conductivity zone; thus, the electron-hole pairs are generated. An electron in the conductivity zone is taken by the oxygen molecules dissolved in suspension, and a hole in the valence zone can be taken by the $OH^-$ particles or the water molecules adsorbed on the catalyst surface to form the hydroxyl radicals.

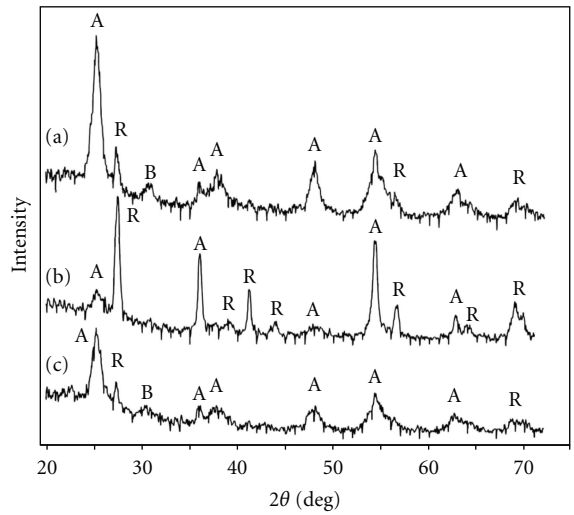


Figure 3: XRD patterns of $TiO_2$-P123 (a), $TiO_2$-PEI (b), and $TiO_2$ (c) powders annealed at 400°C for 4 h.

Thus, the catalytic activity depends substantially on the number of electron-hole pairs in $TiO_2$. The larger the number of such pairs formed on the surface of $TiO_2$, the higher the photocatalytic activity in the process of depigmentation [23]. The number of electron-hole pairs depends on the optical properties of samples. The longer the wavelength of the radiation a sample is capable to absorb under identical radiation conditions, the more the number of electron-hole pairs formed on a surface. Absorption of light below 370 nm is due to the excitation of electrons from the valence band to the conduction band of $TiO_2$. Pure anatase crystalline powder has an intense absorption band in the interval 300–335 nm [24]. A red shift of the absorption edge also indicates a decrease in the band gap of $TiO_2$ in the case of $TiO_2$-P123 film. The use of polyethylenimine, on the contrary, increases the width of the band gap, preventing electron-hole pairs from formation and, as a consequence, leads to a decrease in photocatalytic activity. This fact is probably related to the various phase compositions of the synthesized samples.

*3.2. Crystalline Structure and Morphology.* Typical XRD diffraction patterns of calcinated $TiO_2$ powder are shown in Figure 3.

Crystallization of anatase and brookite already occurs at room temperature, resulting in very fine crystallite size [25]. Brookite ($B$) was observed at very low concentration on samples of $TiO_2$-P123 and $TiO_2$ calcinated at 400°C. The strongest peaks detected for anatase ($A$) and rutile ($R$) were $2\theta = 25.4$ and $2\theta = 27.4$, respectively. The $TiO_2$-PEI sample has more intense rutile peaks (Figure 3(b)). In the other samples, anatase preponderates. The formation of rutile phase together with the anatase phase was found as a result of the peptization achieved by HCl. When powders were annealed, the dehydroxylation generated lattice defects that produced microstrains and created conditions for rearrangement of parallel octahedron in the case of anatase (octahedra connected at their vertices) to 90°-rotated octahedron in the case of rutile (octahedra connected at their edges). Therefore, phase transformation from anatase to rutile can be regarded in terms of reconstructive polymorphism with symmetry change [26].

Based on (2), 400°C-annealed $TiO_2$ powder showed 59% anatase and 41% rutile $TiO_2$ phase with the average crystallite size of 5.6 and 7.5 nm, respectively (Figure 3(a)). The addition of templates alters the phase composition of materials. Polyethylenimine increases the content of the rutile phase (64%) and decreases that of anatase (36%). The crystallite size is also thereby increased to 22.3 and 28.8 nm, respectively. On the other hand, the addition of nonionogenic surfactant Pluronic P-123 decreases the content of the rutile phase (24%) and increases that of anatase (76%) (Figure 3(c)). The crystallite size is also thereby decreased to 5.2 and 3.1 nm. Pluronic P-123 was therefore found to have the biggest impact by the greatest retardation of the formation of the rutile phase and by producing the smallest size of anatase nanocrystals.

Atomic force microscopy (AFM) was employed to characterize the surface morphology of the manufactured samples.

$TiO_2$ powders made without surfactant addition in the sol exhibit a flat and ill-defined surface (Figure 4(b)), whereas $TiO_2$ made with polyethylenimine addition in the sol (Figure 4(a)) exhibits a rougher but still moderately flat texture and well-structured granular nanosurface with clear interstices between the particles/aggregates. Crystallite sizes obtained from XRD measurements are only roughly comparable to the particle size obtained from AFM analysis. Particle size distribution is broader comparing to the $TiO_2$ sample with maximum at 15 nm. The use of Pluronic P-123, in its turn, makes it possible to obtain the materials with more highly developed surface. Crystallite sizes obtained from XRD measurements (7 nm) are in a good agreement with AFM analysis (Figure 4(c)). The use of Pluronic P-123 makes it possible to obtain the materials with very narrow size distribution. The well-structured morphology displayed in the AFM image of powders dosed with a template is likely a consequence of template removal during the thermal treatment. It creates a higher degree of porosity, which should have a beneficial influence on the photocatalytic activity of the materials dosed with a template provided that the pores are accessible for an organic pollutant. The physisorption measurements revealed that the Hombikat industrial sample showed wide range of pore size distribution. All samples synthesized from titania hydrosols exhibit mesoporous structure.

The hysteresis loop (Figure 5(a)) in the adsorption-desorption isotherms of the $TiO_2$ sample indicated the pores in the sample were bottle-neck type (type E). The specific surface area of the $TiO_2$ sample was 74 $m^2$/g with pore volume of 0.105 $m^3$/g (Table 1). The $TiO_2$-PEI sample showed wide range of pore size distribution (3–60 nm) with peak at 11.3 nm (Figure 5(b)). In the case of $TiO_2$-P123 sample, the pore size distribution was narrow and varied from 2 to 20 nm with the peak at 12.4 nm (Figure 5(c)). The pore volume of the sample was 0.328 $m^3$/g, with the specific surface area of 105 $m^2$/g. The hysteresis obtained from the sorption analysis

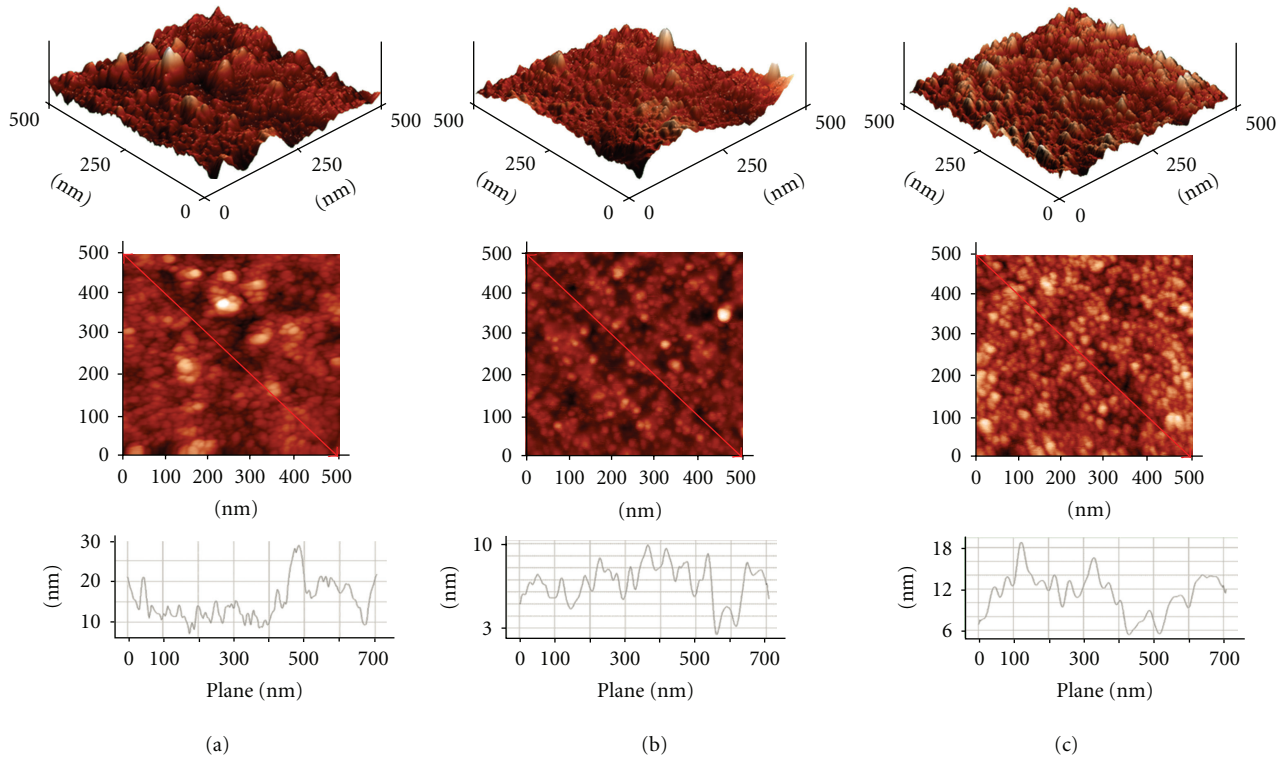


Figure 4: AFM images and particle size distribution of the calcinated samples: $TiO_2$-PEI (a), $TiO_2$ (b), and $TiO_2$-P123 (c).

Table 1: Characteristics of the mesoporous titania samples.

| Sample name | [a]BET ($m^2\ g^{-1}$) | [b]$S_{mesopor}$ ($m^2/g$) | [c]$V_p$ ($cm^3/g$) | [d]$D_p$ (nm) |
|---|---|---|---|---|
| $TiO_2$ | 74 | 97 | 0.105 | 5.7 |
| $TiO_2$-P123 | 105 | 122 | 0.328 | 12.4 |
| $TiO_2$-PEI | 63 | 64 | 0.177 | 11.3 |
| Hombikat | 51 | 36 | 0.456 | >1000 |

[a]The BET surface areas were calculated using the BET equation.
[b]The mesoporous surface areas were calculated using the BJH equation on the desorption branches of the isotherms.
[c]Total pore volume determined by BJH at $p/p_0$ ratio of 0.988.
[d]Average pore diameter.

of the sample (Figure 5(c)) also showed formation of bottle type pores.

However, the ratio of body to neck diameter decreased from the $TiO_2$ sample to the $TiO_2$-P123 sample. The hysteresis loop of the adsorption-desorption isotherms of $TiO_2$-PEI (Figure 5(b)) indicated formation of cylindrical pores (type A). Formation of pores with different morphology clearly demonstrated the role of the templates in engineering the pore structure, as titania sol is otherwise known to form anatase and rutile with bottle-neck-type pores in the absence of any structure-directing template.

*3.3. Photodegradation.* Photocatalytic activity of samples was estimated using the reaction of decomposition of methyl orange ([4[[4-dimethylaminophenyl]-azo]benzenesulfonic acid sodium salt] with the molecular formula $[(CH_3)_2NC_6H_4NNC_6H_4SO_3Na]$) in water solutions. Before exposure to irradiation, samples were stirred in the darkness for half an hour. The measurements indicate a negligibly small decrease in the concentration of methyl orange caused by its insignificant adsorption on the catalyst surface. Thus, in the absence of irradiation, decomposition does not occur.

The methyl orange concentration change versus time of UV-light irradiation is shown in Figure 6.

The results reveal that photocatalytic decomposition of methyl orange can be described using the pseudo-first-order kinetic model: $\ln(C_0/C) = kt$. As is known, the photocatalytic activity of catalysts is affected by some factors, such as textural properties of a material, crystal structure, phase composition, and electron-hole pair recombination rate.

It is well seen and that the $TiO_2$-P123 sample has shown high rates of decomposition of model dye in comparison to the other samples. The solution of dye with $TiO_2$-P123 was completely decolorized in 30 min. The rate constant increases considerably from $5.82 \cdot 10^{-2}\ min^{-1}$ to $1.49 \cdot 10^{-1}\ min^{-1}$ with application of template addition.

The high magnitude of rate constant at $1.49 \cdot 10^{-1}\ min^{-1}$ shows that application of such template as Pluronic P-123 accelerates the process of decomposition of methyl orange model dye due to the large surface area ($105\ m^2/g$) and decrease in the crystallite size, that is, increase in surfacially active zone, and also due to narrow pore size distribution. Apparently, this additive leads to an increase in the number of formed electron-hole pairs. The crystal structure substantially affects the photocatalytic activity of $TiO_2$. Many researchers have confirmed that the anatase

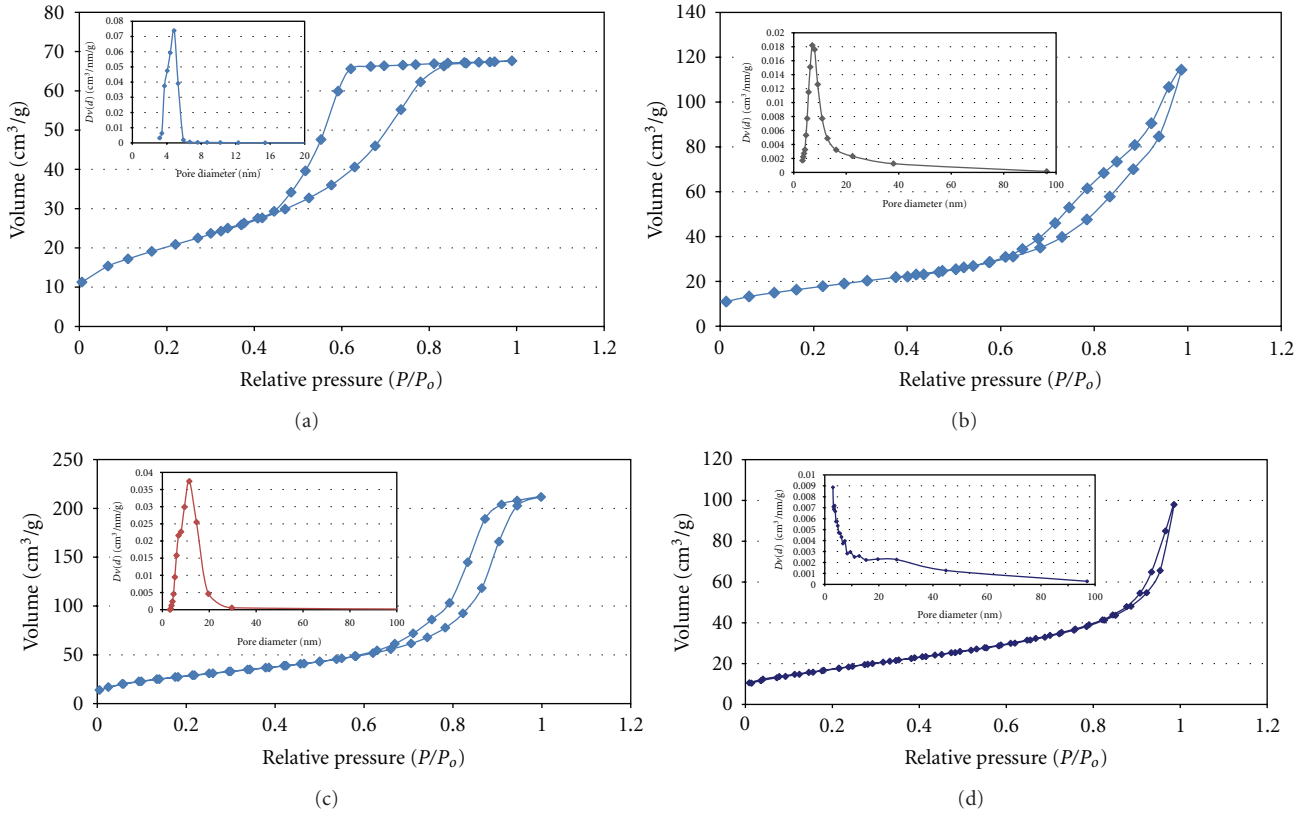


Figure 5: Nitrogen adsorption/desorption isotherms with the corresponding pore size distribution curves of mesoporous titania samples after calcination: (a) $TiO_2$, (b) $TiO_2$-PEI, (c) $TiO_2$-P123, and (d) Hombikat.

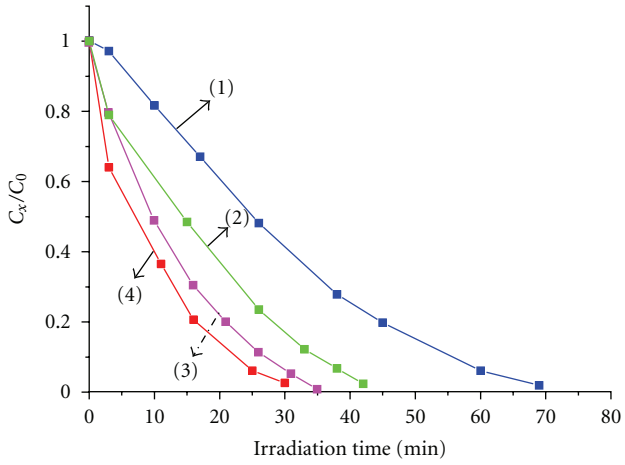


(1) $TiO_2$-PEI
(2) $TiO_2$
(3) Hombikat
(4) $TiO_2$-P123

Figure 6: Photodegradation of methyl orange under UV irradiation.

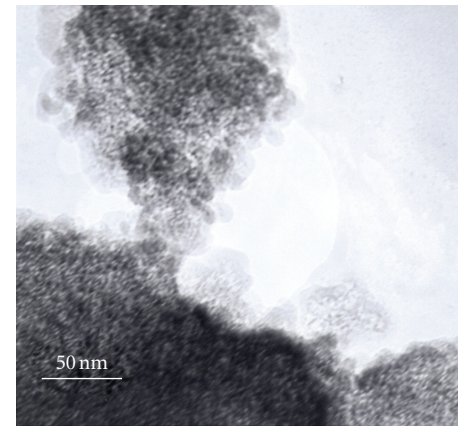


Figure 7: TEM image of the $TiO_2$-P123 sample.

phase has higher photocatalytic reactivity than the rutile phase [27]. This distinction can be related to oxidation and reduction of photogenerated holes and electrons in the conductivity zone and the valence zone in the phase of anatase and rutile. Besides, the photocatalytic activity of individual anatase and rutile crystal phases is considered to be much lower as compared to the materials involving their combination [28–30]. Possibly, $TiO_2$-P123 has optimum structure of crystal phases of anatase (76%) and rutile (24%) and optimum porous structure (Figure 7), which also promotes the increase in its photocatalytic activity.

Photocatalytic activity of the materials modified with Pluronic P-123 is superior to that of commercial Hombikat

photocatalyst. Low photoactivity was found for the sample with the addition of PEI. This fact is probably related to its phase composition since one can observe a prevalence of the rutile phase that is known to decrease the photocatalytic activity because of a decrease in recombination of photogenerated electrons and holes, and the decrease is also related to the small surface area (63 $m^2/g$) and wide particle size distribution.

Thus, the photocatalytic activity of titania obtained from hydrosols can be substantially increased by calcinating the mesostructures formed in the presence of nonionogenic surfactant Pluronic P-123.

## 4. Summary

Mesoporous crystalline titanium dioxide materials have been successfully synthesized via a simple and cheap surfactant-assisted sol-gel method using titania hydrosols and different organic templates as starting materials. Pure $TiO_2$ powder showed 59% anatase and 41% rutile $TiO_2$ phase with the average crystallite size of 5.6 and 7.5 nm, respectively. The addition of templates alters the phase composition of materials. Polyethylenimine increases the content of the rutile phase (64%) and decreases that of anatase (36%). The crystallite size is also thereby increased to 22.3 and 28.8 nm, respectively. On the other hand, the addition of nonionogenic surfactant Pluronic P-123 decreases the content of the rutile phase (24%) and increases that of anatase (76%) (Figure 3(c)). The crystallite size is also thereby decreased to 5.2 and 3.1 nm. Pluronic was therefore found to have the biggest impact by the greatest retardation of the formation of the rutile phase and by producing the smallest size of anatase nanocrystals. Formation of pores with different morphology clearly demonstrated the role of the templates in engineering the pore structure. Application of polyethylenimine leads to the formation of cylindrical pores. The hysteresis loop in the adsorption-desorption isotherms of the $TiO_2$ and $TiO_2$-P123 samples indicated the pores in the samples were of bottle-neck type. In the process of photodegradation of methyl orange, the photocatalytic activity of materials modified with Pluronic P-123 is superior to that of all synthesized systems and commercial Hombikat photocatalyst. The $TiO_2$-P123 sample has the optimum composition of crystalline phases of anatase and rutile, which promotes the increase in its photocatalytic activity.

## Acknowledgments

This work is supported by RFBR Grants no. 09-03-97553, 11-03-12063-ofi, 12-03-97538, joint RFBR-DST Grant 10-03-92658, and the Grant of the Russian Ministry of Education and Science no. 14.740.12.0862.

## References

[1] B. O'Regan and B. M. Grätzel, "A low-cost, high-efficiency solar cell based on dye-sensitized colloidal $TiO_2$ films," *Nature*, vol. 353, no. 6346, pp. 737–740, 1991.

[2] M. A. Fox and M. T. Dulay, "Heterogeneous photocatalysis," *Chemical Reviews*, vol. 93, no. 1, pp. 341–357, 1993.

[3] A. L. Linsebigler, G. Lu, and J. T. Yates, "Photocatalysis on $TiO_2$ surfaces: principles, mechanisms, and selected results," *Chemical Reviews*, vol. 95, no. 3, pp. 735–758, 1995.

[4] D. S. Bhatkhande, V. G. Pangarkar, and A. A. C. M. Beenackers, "Photocatalytic degradation for environmental applications—a review," *Journal of Chemical Technology and Biotechnology*, vol. 77, no. 1, pp. 102–116, 2002.

[5] O. Carp, C. L. Huisman, and A. Reller, "Photoinduced reactivity of titanium dioxide," *Progress in Solid State Chemistry*, vol. 32, no. 1-2, pp. 33–177, 2004.

[6] K. Hashimoto, H. Irie, and A. Fujishima, "$TiO_2$ photocatalysis: a historical overview and future prospects," *Japanese Journal of Applied Physics 1*, vol. 44, no. 12, pp. 8269–8285, 2005.

[7] D. Mao, G. Lu, and Q. Chen, "Influence of calcination temperature and preparation method of $TiO_2$-$ZrO_2$ on conversion of cyclohexanone oxime to $\varepsilon$-caprolactam over $B_2O_3$/$TiO_2$-$ZrO_2$ catalyst," *Applied Catalysis A*, vol. 263, no. 1, pp. 83–89, 2004.

[8] R. Fretwell and P. Douglas, "An active, robust and transparent nanocrystalline anatase $TiO_2$ thin film—preparation, characterisation and the kinetics of photodegradation of model pollutants," *Journal of Photochemistry and Photobiology A*, vol. 143, no. 2-3, pp. 229–240, 2001.

[9] B. E. Yoldas, "Hydrolysis of titanium alkoxide and effects of hydrolytic polycondensation parameters," *Journal of Materials Science*, vol. 21, no. 3, pp. 1087–1092, 1986.

[10] J. Yu, X. Zhao, and Q. Zhao, "Effect of surface structure on photocatalytic activity of $TiO_2$ thin films prepared by sol-gel method," *Thin Solid Films*, vol. 379, no. 1-2, pp. 7–14, 2000.

[11] J. Yu, X. Zhao, J. Du, and W. Chen, "Preparation, microstructure and photocatalytic activity of the porous $TiO_2$ anatase coating by sol-gel processing," *Journal of Sol-Gel Science and Technology*, vol. 17, no. 2, pp. 163–171, 2000.

[12] D. J. Kim, S. H. Hahn, S. H. Oh, and E. J. Kim, "Influence of calcination temperature on structural and optical properties of $TiO_2$ thin films prepared by sol-gel dip coating," *Materials Letters*, vol. 57, no. 2, pp. 355–360, 2002.

[13] C. Legrand-Buscema, C. Malibert, and S. Bach, "Elaboration and characterization of thin films of $TiO_2$ prepared by sol–gel process," *Thin Solid Films*, vol. 418, no. 2, pp. 79–84, 2002.

[14] L. Zhang, Y. Zhu, Y. He, W. Li, and H. Sun, "Preparation and performances of mesoporous $TiO_2$ film photocatalyst supported on stainless steel," *Applied Catalysis B*, vol. 40, no. 4, pp. 287–292, 2003.

[15] S. Bu, Z. Jin, X. Liu, L. Yang, and Z. Cheng, "Fabrication of $TiO_2$ porous thin films using peg templates and chemistry of the process," *Materials Chemistry and Physics*, vol. 88, no. 2-3, pp. 273–279, 2004.

[16] S. J. Bu, Z. G. Jin, X. X. Liu, L. R. Yang, and Z. J. Cheng, "Synthesis of $TiO_2$ porous thin films by polyethylene glycol templating and chemistry of the process," *Journal of the European Ceramic Society*, vol. 25, no. 5, pp. 673–679, 2005.

[17] B. Guo, Z. Liu, L. Hong, and H. Jiang, "Sol gel derived photocatalytic porous $TiO_2$ thin films," *Surface and Coatings Technology*, vol. 198, no. 1–3, pp. 24–29, 2005.

[18] Y. Djaoued, M. Thibodeau, J. Robichaud et al., "Photocatalytic degradation of domoic acid using nanocrystalline $TiO_2$ thin films," *Journal of Photochemistry and Photobiology A*, vol. 193, no. 2-3, pp. 271–283, 2008.

[19] G. Oskam, A. Nellore, R. L. Penn, and P. C. Searson, "The growth kinetics of $TiO_2$ nanoparticles from titanium(IV) alkoxide at high water/titanium ratio," *The Journal of Physical Chemistry B*, vol. 107, no. 8, pp. 1734–1738, 2003.

[20] D. Vorkapic and T. Matsoukas, "Reversible agglomeration: a kinetic model for the peptization of titania nanocolloids,"

*Journal of Colloid and Interface Science*, vol. 214, no. 2, pp. 283–291, 1999.

[21] R. A. Spurr and H. Myers, "Quantitative analysis of anatase-rutile mixtures with an X-ray diffractometer," *Analytical Chemistry*, vol. 29, no. 5, pp. 760–762, 1957.

[22] M. C. Cordero-Cabrera, G. S. Walker, and D. M. Grant, "Effect of processing parameters on the particle size and stabilisation of titania sols," *Journal of Materials Science*, vol. 40, no. 14, pp. 3709–3714, 2005.

[23] Y. Gou, D. Chen, and Z. X. Su, "Photocatalyst of nanometer $TiO_2$/conjugated polymer complex employed for depigmentation of methyl orange," *Applied Catalysis A*, vol. 261, no. 1, pp. 15–18, 2004.

[24] H. Yoshitake, T. Sugihara, and T. Tatsumi, "Preparation of wormhole-like mesoporous $TiO_2$ with an extremely large surface area and stabilization of its surface by chemical vapor deposition," *Chemistry of Materials*, vol. 14, no. 3, pp. 1023–1029, 2002.

[25] M. R. Mohammadi, M. C. Cordero-Cabrera, M. Ghorbani, and D. J. Fray, "Synthesis of high surface area nanocrystalline anatase-$TiO_2$ powders derived from particulate sol-gel route by tailoring processing parameters," *Journal of Sol-Gel Science and Technology*, vol. 40, no. 1, pp. 15–23, 2006.

[26] X. Bokhimi, A. Morales, and F. Pedraza, "Crystallography and crystallite morphology of rutile synthesized at low temperature," *Journal of Solid State Chemistry*, vol. 169, no. 2, pp. 176–181, 2002.

[27] S. Kim and S. H. Ehrman, "Photocatalytic activity of a surface-modified anatase and rutile titania nanoparticle mixture," *Journal of Colloid and Interface Science*, vol. 338, no. 1, pp. 304–307, 2009.

[28] X. F. Zhou, D. B. Chu, S. W. Wang, C. J. Lin, and Z. Q. Tian, "New route to prepare nanocrystalline $TiO_2$ and its reaction mechanism," *Materials Research Bulletin*, vol. 37, no. 11, pp. 1851–1857, 2002.

[29] T. Ohno, K. Tokieda, S. Higashida, and M. Matsumura, "Synergism between rutile and anatase $TiO_2$ particles in photocatalytic oxidation of naphthalene," *Applied Catalysis A*, vol. 244, no. 2, pp. 383–391, 2003.

[30] S. Bakardjieva, J. Šubrt, V. Štengl, M. J. Dianez, and M. J. Sayagues, "Photoactivity of anatase-rutile $TiO_2$ nanocrystalline mixtures obtained by heat treatment of homogeneously precipitated anatase," *Applied Catalysis B*, vol. 58, no. 3-4, pp. 193–202, 2005.